INORGANIC CHEMISTRY
FRONTIERS

RESEARCH ARTICLE

View Article Online
View Journal | View Issue

Cite this: *Inorg. Chem. Front.*, 2022, **9**, 2336

Synthesis and structures of fluoride-bridged dysprosium clusters: influence of fluoride ions on magnetic relaxation behaviors†

Qiong Yuan,[a] Yin-Shan Meng,[b] Yi-Quan Zhang,[c] Chen Gao,[a] Shan-Shan Liu,[d] Bing-Wu Wang *[a] and Song Gao *[a,e]

The synthesis of fluoride-bridged tri-([{Cp′$_2$Dy}{μ-F}]$_3$·tol, **1Dy**, Cp′ = $C_5H_4Si(CH_3)_3$; tol = toluene), tetra-([{Cp′$_2$Dy(μ-F)$_2$}$_2${(Cp′)(THF)Dy(μ-F)}$_2$]·hex, **2Dy**, THF = tetrahydrofuran; hex = *n*-hexane), and hepta-nuclear (**3Dy**) dysprosium complexes is reported here and a hydroxy-bridged dinuclear dysprosium complex [Cp′$_2$Dy(μ-OH)]$_2$(**4Dy**) is synthesized for comparison. The nucleation number of the fluoride-bridged complexes highly depends on the reaction solvents and the molar ratio of the dysprosium and fluoride precursors. The three Dy ions in **1Dy** are arranged in a triangular fashion and the tetranuclear **2Dy** displays a butterfly shape geometry. **3Dy** shows a much more complicated structure with three types of fluoride bridges. **1Dy** and **2Dy** exhibit slow relaxation of magnetization with the energy barriers of 95 K and 98 K, respectively, while the dinuclear and heptanuclear dysprosium complexes barely show any behaviors of molecular nanomagnets. *Ab initio* calculations demonstrated that the thermo-assisted relaxation of magnetization of **1Dy** and **2Dy** originated from the {Cp′$_2$Dy} fragment. Analysis of magneto-structural correlation revealed that the fluoride ions had a great influence on the orientation of the easy axis of magnetization and the exchange interactions.

Received 11th November 2021,
Accepted 5th March 2022

DOI: 10.1039/d1qi01422f

rsc.li/frontiers-inorganic

Introduction

Recently, polynuclear lanthanide clusters possessing diverse structures and topologies have attracted increasing interest in coordination chemistry, owing to not only the fundamental pursuit of complicated and novel structures but also the challenging synthesis, interesting physical properties and potential applications.[1–4] Compared with transition metal ions, the orbital angular momentum of 4f metal ions is largely conserved due to the localization of 4f electrons near the nucleus and hence there is no significant perturbation from the ligand field.[5] Thus, the 4f metal ions exhibit much stronger spin–orbit coupling. The large magnetic anisotropy of lanthanide ions makes them ideal candidates for synthesizing single-molecule magnets (SMMs).[6–10] With respect to the molecular nanomagnets, great efforts have been made in understanding and fine-tuning the uniaxial magnetic anisotropy and exchange interactions in order to generate high barriers for spin-reversal. So far, the highest barriers and blocking temperatures have been realized in dysprosium single-ion magnets (Dy-SIMs).[11–15] In light of the lack of progress in multinuclear Dy-SMMs, we explore the effect of the nucleation number and exchange interactions on the magnetic relaxation of Dy-SMMs in this work.

A panoply of lanthanide clusters with a variety of core motifs and nucleation numbers have been successfully synthesized with widely used bridging ligands such as carboxylates,[16–18] phosphates,[19] sulfonates,[20] nitronylnitroxide radicals,[21–24] halides,[25–29] *etc.*[30] It is known that the fluoride ion possesses a smaller ionic radius and larger electronegativity than the N and O atoms. Therefore, the F ion in the terminal Dy–F bond is believed to provide stronger crystal field splitting and stabilize the $|M_J|$ = 15/2 ground state of Dy, as

[a]*Beijing National Laboratory of Molecular Science, State Key Laboratory of Rare Earth Materials Chemistry and Applications, Beijing Key Laboratory for Magnetoelectric Materials and Devices, Peking University, College of Chemistry and Molecular Engineering, Peking University, Beijing 100871, P. R. China*
[b]*State Key Laboratory of Fine Chemicals, Dalian University of Technology, 2 Linggong Rd., Dalian 116024, P. R. China*
[c]*Jiangsu Key Laboratory for NSLSCS, School of Physical Science and Technology, Nanjing Normal University, Nanjing 210023, P. R. China*
[d]*Beijing Key Laboratory of Fuels Cleaning and Advanced Catalytic Emission Reduction Technology, College of Chemical Engineering, Beijing Institute of Petrochemical Technology, Beijing 102617, PR China*
[e]*School of Chemistry and Chemical Engineering, South China University of Technology, Guangzhou 510640, P. R. China*

†Electronic supplementary information (ESI) available: Additional computational details and magnetic and crystallographic data are provided in the ESI. CCDC 2121103, 2121109, 2121120 and 2121121 for compounds **1Dy–4Dy**. For ESI and crystallographic data in CIF or other electronic format see DOI: https://doi.org/10.1039/d1qi01422f

predicted by Liviu Ungur and co-workers.[31] The recent work by Norel and co-workers[28] rationalized this theoretical prediction by showing that the terminal fluoride complex [Dy(Tp^{py})F(dioxane)][PF_6] (Tp^{py} = tris(3-(2-pyridyl)pyrazolyl)hydroborate) exhibits a high spin-reversal barrier of 432 cm^{-1}. We are also curious about the effects of fluoride ions on the magnetic properties of multifluorido lanthanide complexes where small F bridges can also shorten the distance between two Dy ions and may reinforce the magnetic interactions between them. However, pure fluoride-bridged lanthanide complexes are very limited because the highly insoluble LnF_3 can be easily formed. Most of the reported fluoride-bridged complexes are transition metals and 3d–4f species. The synthesis of fluoride-bridged lanthanide clusters needs careful control of multifluorido lanthanide cores to avoid the formation of LnF_3. Besides, the introduction of fluoride ions using suitable fluoride precursors is also challenging as most of the fluoride salts are insoluble in organic solvents. The fluoride precursor Et_3N·HF caught our attention as it can dissolve in THF easily. It also provides good reactivity with lanthanide metallocenes. In this work, we chose [Cp′$_3$Dy] to react with Et_3N·HF and obtained several clusters with varied numbers of Dy ions through changing different solvents or different molar ratios of reactants. The hydroxide-bridged complex **4Dy** was also prepared using a similar method to compare the effects of hydroxide and fluoride bridges on their magnetic properties.

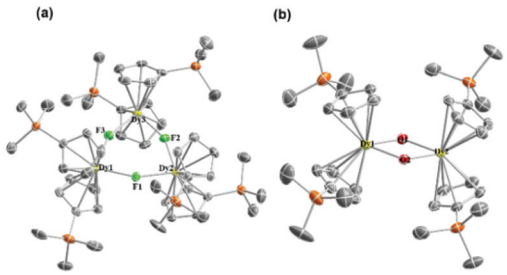

Fig. 1 Molecular structures of **1Dy** (a) and **4Dy** (b). Co-crystallized THF and toluene and hydrogens are omitted for clarity. Color code: C, grey; Dy, yellow; Si, light orange; O, red; and F, green.

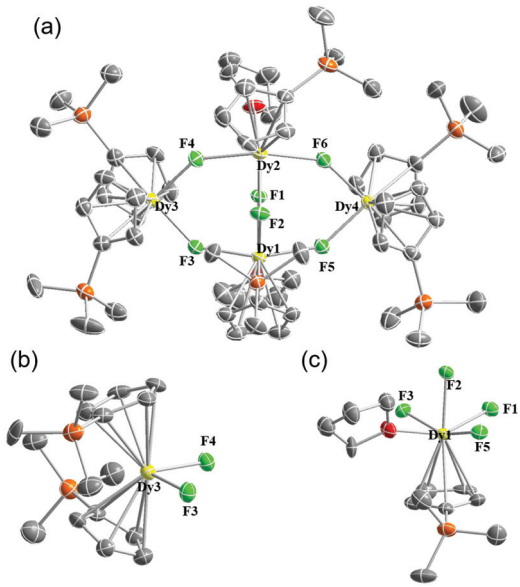

Fig. 2 Molecular structures of **2Dy**. Co-crystallized THF and toluene and hydrogens are omitted for clarity. Color code: C, grey; Dy, yellow; Si, light orange; O, red; and F, green.

Results and discussion

Synthesis and structural characterization

The synthesis of fluoride-bridged dysprosium clusters was performed by adding an equivalent of Et_3N·HF into a cold THF solution of [Cp′$_3$Dy] very slowly. After filtering and removing the solvent, the raw products crystallizing in toluene and hexane could result in two different complexes **1Dy** [Cp′$_2$Dy(μ-F)]$_3$·tol and **2Dy**[{Cp′$_2$Dy(μ-F)$_2$}$_2${(Cp′)(THF)Dy(μ-F)}$_2$]·hex. The reaction is promoted by the protonation of the Cp′ anion. The protonation degree depends highly on the crystallizing solvent and molar ratio of Et_3N·HF and [Cp′$_3$Dy] (see the ESI† Experimental section). An X-ray diffraction experiment indicated that **1Dy** and **2Dy** crystallize in the space group of $P\bar{1}$ and $P2_1/c$, respectively. Their molecular structures are shown in Fig. 1 and 2, respectively.

Complex **1Dy** possesses a typical cyclic trimer structure. The three [Cp′$_2$Dy]$^+$ motifs are connected by μ-F bridges in a triangular manner. Each motif possesses very similar structural parameters, as listed in Table S2.† Each Dy^{III} ion is coordinated by two Cp′ anions and bridged by two fluoride ions with the other two Dy^{III} ions. The Dy–F bond lengths fall in a narrow range of 2.194(2)–2.204(2) Å. The Dy–C bond lengths are in a relatively broader range of 2.630(5)–2.721(5) Å. The Dy^{III} ions and F$^-$ ions are almost within a plane. The structurally related **4Dy** is a dinuclear complex, wherein the [Cp′$_2$Dy]$^+$ motifs are connected by two hydroxide bridges (Dy–O: 2.232(2)–2.261(2) Å). The specific bond length and bond angle information is listed in Table S5.†

Complex **2Dy** is obtained in the hexane solution and crystallizes with a highly disordered hexane molecule in the unit cell. The tetranuclear complex adopts a chair-like structure, in which the Dy^{III} ions can be divided into two kinds. In **2Dy**, there are four Dy^{III} ions and four fluoride ions composed of an eight-membered ring. Dy3 and Dy4 ions are coordinated by two Cp′ anions (Dy–C: 2.64(1)–2.69 Å) and two bridging fluoride ions (Dy–F: 2.172(5)–2.199(6) Å). The angles for F3–Dy3–F4 and F5–Dy4–F6 are 90.6° and 88.4°, respectively, which are slightly larger than those in **1Dy** (85.9°–87.5°). Within the Dy3 and Dy4 metallocenes, one of the Dy–F bonds shows a smaller distance. Both Dy1 and Dy2 ions coordinate with only one Cp′ ring, one THF (Dy–C: 2.68(1)–2.72(1) Å), Dy–O: 2.396(7)–2.409(6) Å) and four bridged fluoride ions (Dy–F: 2.204(5)–2.267(5) Å). Dy1 and Dy2 are further bridged by two fluoride ions.

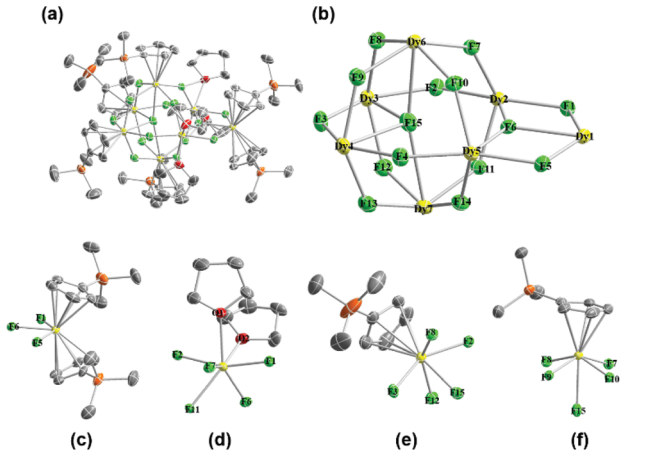

Fig. 3 Molecular structures of **3Dy** (a) and the core of **3Dy** (b); the local coordination environments for Dy1, Dy2, Dy3 and Dy4 are shown in (c) (d), (e) and (f), respectively. Co-crystallized THF and toluene and hydrogens are omitted for clarity. Color code: C, grey; Dy, yellow; Si, light orange; O, red; and F, green.

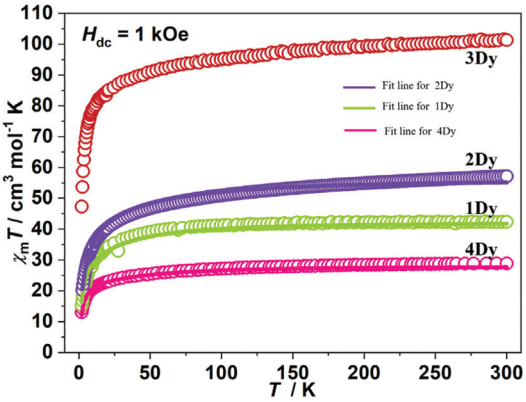

Fig. 4 Susceptibility temperature product $\chi_m T$ as a function of temperature recorded on samples of **1Dy**, **2Dy**, **3Dy** and **4Dy** in an applied field of 1 kOe. The solid line represents the simulation from CASSCF POLY_ANISO calculated results.

When the molar ratio of [Cp′$_3$Dy] and Et$_3$N·HF was changed to 1 : 1.5, a structurally more complicated heptanuclear dysprosium core **3Dy** ($C_{64}H_{110}Dy_7F_{15}O_4Si_6$·hex) was obtained. Five Dy^{III} ions and five fluoride ions form a ten-membered ring with two Dy^{III} ions locating on the two sides of the plane. The Dy^{III} ions in the heptanuclear core can be divided into four kinds (Fig. 3). The Dy1 motif (Fig. 3c) is composed of two Cp′ anions (Dy–C: 2.671(5)–2.690(5) Å) and three fluoride ions (Dy–F: 2.268(3)–2.340(2) Å). Dy2 and Dy5 ions are coordinated only by fluoride ions (Dy–F: 2.182(2)–2.308(3) Å) and THF molecules (Dy–O: 2.370(5)–2.402(4) Å) without Cp′ rings. Dy3, Dy4, Dy6 and Dy7 ions are all capped by mono-Cp′ anions (Dy–C: 2.629(6)–2.696(6) Å). The difference lies in the central F15 ion being closer to Dy3 and Dy4 (2.515(3) and 2.550(3) Å for Dy3–F15 and Dy4–F15; 2.813(2) and 2.695(2) Å for Dy6–F15 and Dy7–F15). As can be seen, through fine-tuning the reaction and crystallizing conditions in the {Cp′$_3$Dy + Et$_3$N·HF} system, we can obtain well-defined Cp′–Dy–F clusters with various numbers of Dy ions. The diverse structures also highlight the versatility of fluoride ions as bridging ions to offer rich coordination chemistry.

Magnetic properties

The variety of dysprosium cores provides a good platform to investigate the impact of fluoride ions on their magnetic properties. The direct current (dc) magnetic susceptibility measurements were performed between 2 K and 300 K under a 1 kOe applied dc field. At room temperature, the $\chi_m T$ values for the four complexes are 28.93, 42.34, 57.19 and 101.29 cm^3 mol^{-1} K, as shown in Fig. 4, which are in good agreement with the calculated values for the uncoupled Dy^{3+} ions (for one free Dy the value is 14.17 cm^3 mol^{-1} K). Upon cooling, the $\chi_m T$ values of the four complexes decrease slowly and begin to decrease rapidly below 25 K. At 2 K, the $\chi_m T$ values are 13.07, 15.28, 20.19 and 47.31 cm^3 mol^{-1} K, respectively, which are all less than half of their initial values at room temperature. Such a decrease is probably caused by the thermal depopulation of the Stark levels. The intramolecular antiferromagnetic interaction could also lead to a decrease of $\chi_m T$ values and would be more predominant below 25 K. Field-dependent magnetization data were collected from 0 to 50 kOe at selected temperatures (see ESI Fig. S1–S4†). At 2 K, the magnetization values for the four complexes increase steeply at low fields and finally reach 10.51, 15.76, 20.34 and 37.96 Nβ at 50 kOe, respectively, which are comparable to the magnetization value per Dy^{III} ion (4.7–5.3 Nβ). The non-superposition of the *M versus* HT^{-1} plots suggests the presence of magnetic anisotropy.

To further investigate the effects of fluoride ions on the slow magnetic relaxation, alternating current (ac) susceptibility measurements were performed in the frequency range of 100–10 000 Hz. For **1Dy**, measurements of ac susceptibilities conducted in the absence of a dc field showed frequency-dependent signals between 2 K and 10 K (Fig. 5a). This result clearly indicates the slow relaxation of magnetization, a behavior of the SMMs. It is worth noting that below 4 K (Fig. S5†), χ''_m surges up to significantly high values, suggesting a very fast relaxation rate above 10^4 Hz. This fast relaxation behavior was also previously observed in a cyclic dysprosium tetramer[32] and was possibly caused by thermally assisted quantum tunneling of magnetization (QTM) *via* the low-lying exchange-coupled excited states. Above 4 K, Cole–Cole plots confirmed a single thermo-related relaxation in the experimental temperature range, with a relatively narrow distribution of relaxation time (α: 0.29–0.08) (see ESI Fig. S8†). The plots of extracted relaxation times τ *versus* T^{-1} show the nonlinearity in the measured temperature range (Fig. 6). Such curvature is probably caused by the low-temperature QTM and other processes. Therefore, Arrhenius fitting cannot be applied to obtain the effective energy barrier. Therefore, the Orbach, Raman and QTM process fitting is introduced to the experimental data points, that is, the fitting formula (1), $\tau^{-1} = 1/\tau_0 \times e^{-U_{eff}/T} + CT^n$

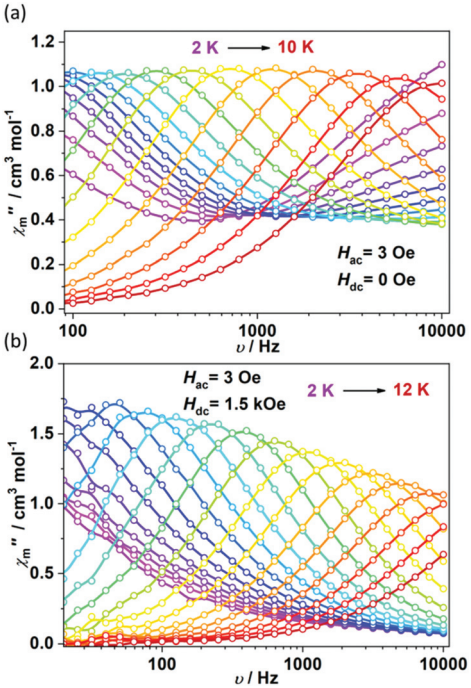

Fig. 5 Plots of out-of-phase susceptibilities (χ''_m) *versus* frequency (υ) for **1Dy**, under a zero applied dc field (a), and under a 1.5 kOe dc field, with an ac field of 3 Oe (b).

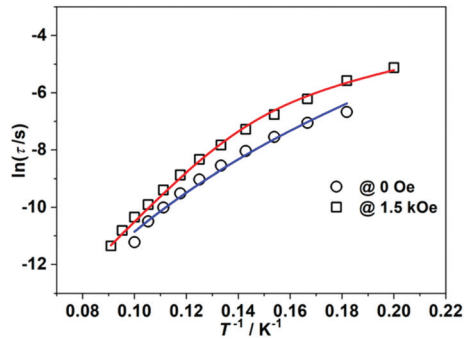

Fig. 6 Plots of the natural logarithm of relaxation time ln(τ) *vs.* T^{-1} for **1Dy** in a zero static field (circle) and 1.5 kOe dc field (square). The solid lines represent the best fit according to the Arrhenius law in the thermally activated regime.

+ $1/\tau_{tunneling}$, yielded an effective energy barrier of U_{eff} = 87 K, a pre-exponential factor $\tau_0 = 3.22 \times 10^{-9}$ s, n = 7.49, C = 0.0017 s^{-1} K^{-n} and $\tau_{tunneling} = 4.23 \times 10^{-5}$ s. To suppress the quantum tunneling, a 1.5 kOe dc field was applied. As shown in Fig. 6 and Fig. S6,† the relaxation rates decreased to some extent. Fitting the data set with eqn (2), $\tau^{-1} = 1/\tau_0 \times e^{-U_{eff}/T} + CT^n$, yielded an effective energy barrier of U_{eff} = 95 K, a pre-exponential factor $\tau_0 = 2.27 \times 10^{-9}$ s, n = 4.27 and C = 0.186 s^{-1} K^{-n}. The obtained τ_0 is in the typical range expected for molecular nanomagnets. The relatively small value of n is more likely due to the second-order Raman process for Kramers dysprosium ions. The theoretically calculated magnetization blocking barrier is 80 K (55.8 cm^{-1}) (see ESI Table S6 and Fig. S12†), which is close to the experimental results.

Ac susceptibility measurements on **2Dy** indicate the characteristic SMM behavior below 10 K under zero dc field (Fig. 7 and Fig. S7†). The relaxation of magnetization for **2Dy** occurs in a similar temperature range to that for **1Dy** (Fig. S9†). The magnitudes of χ''_m are also comparable with those of **1Dy**. The plot ln τ *versus* T^{-1} still deviates from linearity even in a higher temperature region (Fig. 8). Similarly, using the Orbach, Raman and QTM processes for fitting, we obtained U_{eff} = 89 K, $\tau_0 = 4.47 \times 10^{-9}$ s, n = 8.61, C = 0.00015 s^{-1} K^{-n} and $\tau_{tunneling} = 2.21 \times 10^{-5}$ s. A 2 kOe applied dc field can suppress the fast relaxation process effectively and reduce the relaxation rate.

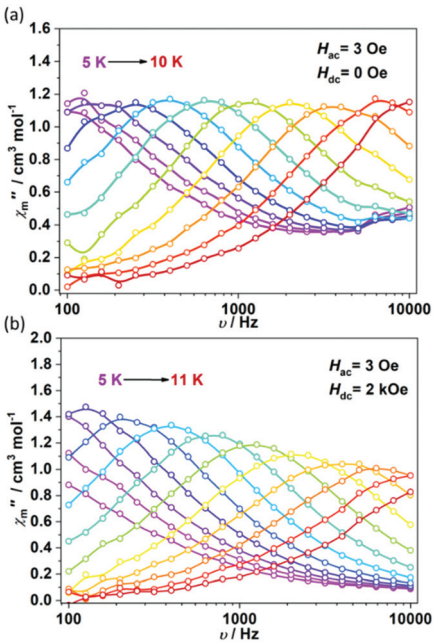

Fig. 7 Out-of-phase signals (χ''_m) *versus* frequency (ν) plots for **2Dy**, under a zero applied dc field (a), and under a 2 kOe dc field, with an ac field of 3 Oe (b).

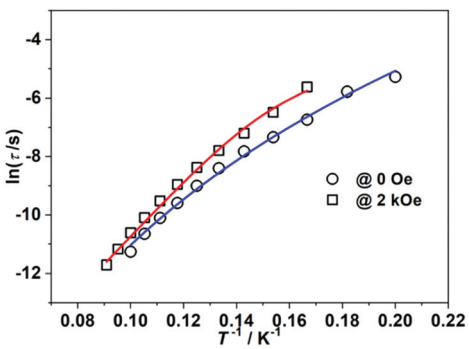

Fig. 8 Plots of the natural logarithm of relaxation time ln(τ) *vs.* T^{-1} for **2Dy** in a zero static field (circle) and a 2 kOe dc field (square). The solid lines represent the best fit according to the Arrhenius law in the thermally activated regime.

The fitting with eqn (1) gives U_{eff} = 97 K, $\tau_0 = 1.38 \times 10^{-9}$ s, n = 3.87 and C = 0.268 s^{-1} K^{-n}, similar to the results for **1Dy**. The results of the theoretical calculations of the magnetization blocking barriers for the four Dy(III) ions in compound **2Dy** are shown in ESI Fig. S13.† The theoretically calculated magnetization blocking barriers for Dy3 and Dy4 (ESI Fig. S13c, d and Table S6†) are 162 K (112.9 cm^{-1}) and 166 K (115.7 cm^{-1}), which are quite different from the experimental results of 97 K. This may be due to the influence of weaker magnetic coupling in the system.

For the heptanuclear **3Dy**, no frequency-dependent resonant χ''_m peaks were observed in any applied fields (see ESI Fig. S10†). As mentioned earlier, the magnetic properties of these compounds mainly depend on the structure of $[Cp_2Dy]^+$ motifs. This is rational as the introduction of additional fluoride ions using $Et_3N{\cdot}HF$ in the coordination spheres of Dy would undermine $[Cp_2Dy]^+$ motifs, which are the origin of the observed magnetic relaxation in **1Dy** and **2Dy** (*vide infra*). For the hydroxide-bridged complex **4Dy**, no frequency-dependent in-phase (χ'_m) and out-of-phase susceptibilities (χ''_m) were observed in the measured temperature range under zero dc field. When a 2.5 kOe dc field was applied, the out-of-phase components showed broad resonant peaks below 3 K (see ESI Fig. S11†). Thus, extracted relaxation times are not restricted due to the lack of well-defined resonant peaks. It can be seen from Fig. S14† that there is an obvious QTM process between the ground double states. The relatively high possibility of QTM between the ground state doublets will quench (accelerate) the relaxation at the initial stage. As a result, compound **4Dy** does not exhibit obvious slow magnetic relaxation behavior under zero field.

Theoretical analysis

Previous study has demonstrated that ancillary ligands within the equatorial plane can greatly affect the slow magnetic relaxation behavior of dysprosium metallocenes.[33] A weak ancillary ligand field would help stabilize the Ising type ground doublet of dysprosium metallocenes. Because of the larger electronegativity and the smaller radii of F than those of O, the interaction between Dy^{III} ions and F^- ions would induce more significant transverse components. However, an ac susceptibility study reveals that **1Dy** and **2Dy** are SMMs while the hydroxide-bridged **4Dy** does not show slow magnetic relaxation behavior within the frequency measurement range of the instrument. To further elucidate the influence of fluoride and hydroxide bridges on their energy levels and magnetic properties, complete-active-space self-consistent field (CASSCF) calculations on individual Dy^{III} fragments for the three complexes on the basis of X-ray determined geometries have been performed with MOLCAS 8.0 and SINGLE_ANISO programs.

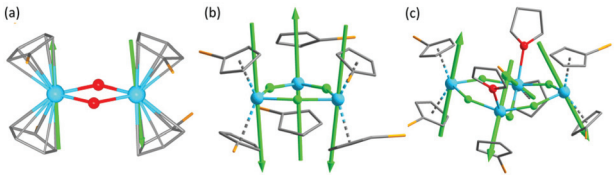

Fig. 9 *Ab initio* calculated (green) magnetic main axes for **4Dy**, **1Dy**, and **2Dy**.

The eight lowest spin–orbit energies and the corresponding g tensors of complexes **4Dy**, **1Dy** and **2Dy** are shown in Table S6.† The calculated ground g_z values of the individual Dy^{III} fragments of **4Dy** are close to 20, and the $g_{x,y}$ values are not negligible. The orientations of easy axes for the cyclic trimer are nearly perpendicular to the plane consisting of the Dy_3F_3 core (Fig. 9b and Fig. S15†), in agreement with the previously reported dysprosium metallocene SMMs. For **2Dy**, the orientations of the two types of Dy^{III} fragments are very different. The Dy3 and Dy4 fragments supported by two Cp′ anions exhibit similar orientations of the easy axis to that in **1Dy**, while the easy axes for Dy1 and Dy2 fragments supported by mono-Cp′ are almost perpendicular to the Cp ring, orienting towards the bridging F2 ion (Fig. 9c and Fig. S16†).

Despite the Dy^{III} fragments except Dy1 and Dy2 in **2Dy** having some deviations from 20, the Lines model was applied to estimate the exchange interactions in **4Dy**, **1Dy** and **2Dy** using the POLY_ANISO[5,13,34–39] program. All parameters in Table 1 were calculated with respect to the pseudospin $\hat{S} = 1/2$ of the Dy^{III} ions corresponding to the Hamiltonian representation in eqn (1)–(3). For complexes **4Dy**, **1Dy** and **2Dy**, the total coupling parameters J (dipolar and exchange) were included to fit the magnetic susceptibilities. The calculated and experimental $\chi_m T$ *versus* T plots of complexes **4Dy**, **1Dy** and **2Dy** are shown in Fig. 4, where the fit for both **4Dy** and **1Dy** is close to

Table 1 Fitted exchange coupling constant J_{exch}, the calculated dipole–dipole interaction J_{dip} and the J between Dy^{III} ions in **4Dy**, **1Dy** and **2Dy** (cm^{-1}). The intermolecular interactions zJ' of the three compounds were set to −0.00 cm^{-1}, −0.06 cm^{-1} and −0.20 cm^{-1}, respectively

	4Dy			**1Dy**			**2Dy**		
	J_{dip}	J_{exch}	J	J_{dip}	J_{exch}	J	J_{dip}	J_{exch}	J
J_1	−2.95	−0.25	−3.18	−1.90	−0.10	−2.00	−1.13	−1.50	−2.63
J_2				−1.86	−0.14	−2.00	−1.10	−1.50	−2.60
J_3				−1.89	3.89	2.00	−0.86	−1.50	−2.36
J_4							0.99	−1.50	−0.51
J_5							5.45	−1.25	4.20

the experimental data. For **2Dy**, however, the fit appeared a little deviated from the experimental data since the individual Dy^{III} fragments of Dy1 and Dy2 cannot be treated as an ideal Ising type considering their ground g_z being relatively far from 20 (see in ESI Table S6†). As seen in Table 1, the Dy⋯Dy interaction in complex **4Dy** within the Lines model[40–42] is antiferromagnetic. For **1Dy**, the Dy1⋯Dy2 and Dy1⋯Dy3 interactions are both antiferromagnetic, while the Dy2–Dy3 interaction is ferromagnetic. For **2Dy**, the Dy1–Dy3, Dy1–Dy4, Dy2–Dy4 and Dy2–Dy3 interactions are all antiferromagnetic, while the Dy2–Dy1 interaction is ferromagnetic. The exchange energies and the main values of g_z for the lowest two exchange doublets for all complexes are given in Table S7.† The g_z values of the ground exchange state for **4Dy**, **1Dy** and **2Dy** are 38.04, 18.48 and 29.75, respectively. Both the experimental and theoretical results demonstrate that introducing more fluoride ions would impair the uniaxial anisotropy of the dysprosium metallocene SMMs. It is more obvious when we refer to the Dy1 fragment in **3Dy** wherein three fluoride ions coordinated to a Dy^{III} ion within the equatorial plane result in the fast relaxation of magnetization.

$$\hat{H}_{\text{exch}} = -J_1\hat{S}_{\text{Dy1}}\hat{S}_{\text{Dy2}} \quad (1)$$

$$\hat{H}_{\text{exch}} = -J_1\hat{S}_{\text{Dy1}}\hat{S}_{\text{Dy2}} - J_2\hat{S}_{\text{Dy1}}\hat{S}_{\text{Dy3}} - J_3\hat{S}_{\text{Dy2}}\hat{S}_{\text{Dy3}} \quad (2)$$

$$\hat{H}_{exch} = -J_1\hat{S}_{\text{Dy1}}\hat{S}_{\text{Dy3}} - J_2\hat{S}_{\text{Dy1}}\hat{S}_{\text{Dy4}} - J_3\hat{S}_{\text{Dy2}}\hat{S}_{\text{Dy3}} - J_4\hat{S}_{\text{Dy2}}\hat{S}_{\text{Dy4}} - J_5\hat{S}_{\text{Dy1}}\hat{S}_{\text{Dy2}} \quad (3)$$

Conclusions

In summary, through systematically tuning the crystallizing solvents and molar ratios of reactants we can obtain three fluoride-bridged tri-, tetra-, and hepta-nuclear Cp-based Dy–F clusters along with a related hydroxy-bridged dinuclear dysprosium complex. The tri- and tetra-nuclear compounds can exhibit slow magnetic relaxation with almost identical energy barriers of 95 and 97 K, while the hydroxide-bridged dinuclear and F-bridged heptanuclear clusters barely display any SMM behavior. *Ab initio* calculations demonstrated that the thermo-assisted relaxation of magnetization arises from the $[Cp'_2Dy(\mu\text{-}F)_2]$ motifs. Through this work on Dy–F clusters, it is rationalized that the fluoride ions mainly affect the orientation of the easy axis and the exchange interactions. In short, for a high-performance single-molecule magnet, the suppression of quantum tunneling through the magnetic interaction of the metal center is an important means to improve the magnetic properties. However, for lanthanide ions, it is also crucial to improve local symmetry.

Conflicts of interest

There are no conflicts to declare.

Acknowledgements

This work is supported by the National Natural Science Foundation of China (21971006, 21621061, 21571008, 22173015 and 21801037), the National Key Basic Research Program of China (2018YFA0306003, 2017YFA0206301 and 2017YFA0204903) and the Natural Science Foundation of Jiangsu Province of China (BK20151542).

Notes and references

1 R. Sessoli, H. L. Tsai, A. R. Schake, S. Wang, J. B. Vincent, K. Folting, D. Gatteschi, G. Christou and D. N. Hendrickson, High-spin molecules: $[Mn_{12}O_{12}(O_2CR)16(H_2O)_4]$, *J. Am. Chem. Soc.*, 1993, **115**, 1804.
2 W. Wernsdorfer and R. Sessoli, Quantum Phase Interference and Parity Effects in Magnetic Molecular Clusters, *Science*, 1999, **284**, 133.
3 D. Gatteschi, R. Sessoli and J. Villain, *Molecular Nanomagnets*, Oxford express, 2006.
4 M. Shiddiq, D. Komijani, Y. Duan, A. Gaita-Ariño, E. Coronado and S. Hill, Enhancing coherence in molecular spin qubits via atomic clock transitions, *Nature*, 2016, **531**, 348.
5 J. D. Rinehart and J. R. Long, Exploiting single-ion anisotropy in the design of f-element single-molecule magnets, *Chem. Sci.*, 2011, **2**, 2078.
6 P. Zhang, Y.-N. Guo and J.-K. Tang, Recent advances in dysprosium-based single molecule magnets: Structural overview and synthetic strategies, *Coord. Chem. Rev.*, 2013, **257**, 1728.
7 D. N. Woodruff, R. E. P. Winpenny and R. A. Layfield, Lanthanide Single-Molecule Magnets, *Chem. Rev.*, 2013, **113**, 5110.
8 Z.-H. Zhu, M. Guo, X.-L. Li and J.-K. Tang, Molecular magnetism of lanthanide: Advances and perspectives, *Coord. Chem. Rev.*, 2019, **378**, 350.
9 R. A. Layfield, Organometallic Single-Molecule Magnets, *Organometallics*, 2014, **33**, 1084.
10 D. Shao and X.-Y. Wang, Development of Single-Molecule Magnets, *Chin. J. Chem.*, 2020, **38**, 1005.
11 F.-S. Guo, B. M. Day, Y.-C. Chen, M.-L. Tong, A. Mansikkamäki and R. A. Layfield, A Dysprosium Metallocene Single-Molecule Magnet Functioning at the Axial Limit, *Angew. Chem., Int. Ed.*, 2017, **56**, 11445.
12 C. A. P. Goodwin, F. Ortu, D. Reta, N. F. Chilton and D. P. Mills, Molecular magnetic hysteresis at 60 kelvin in dysprosocenium, *Nature*, 2017, **548**, 439.
13 J. Liu, Y.-C. Chen, J.-L. Liu, V. Vieru, L. Ungur, J.-H. Jia, L. F. Chibotaru, Y. Lan, W. Wernsdorfer and S. Gao, A Stable Pentagonal Bipyramidal Dy(III) Single-Ion Magnet with a Record Magnetization Reversal Barrier over 1000 K, *J. Am. Chem. Soc.*, 2016, **138**, 5441.
14 S. K. Gupta, T. Rajeshkumar, G. Rajaraman and R. Murugavel, An air-stable Dy(iii) single-ion magnet with high anisotropy barrier and blocking temperature, *Chem. Sci.*, 2016, **7**, 5181.

15 F.-S. Guo, B. M. Day, Y.-C. Chen, M.-L. Tong, A. Mansikkamäki and R. A. Layfield, Magnetic hysteresis up to 80 kelvin in a dysprosium metallocene single-molecule magnet, *Science*, 2018, **362**, 1400.
16 I. A. Gass, B. Moubaraki, S. K. Langley, S. R. Batten and K. S. Murray, A π–π 3D network of tetranuclear μ_2/μ_3-carbonato Dy(iii) bis-pyrazolylpyridine clusters showing single molecule magnetism features, *Chem. Commun.*, 2012, **48**, 2089.
17 G. Brunet, E. Sebastiao, T. G. Witkowski, L. Korobkov, B. Gabidullin and M. Murugesu, A nitrogen-rich ligand as a scaffold for slow magnetic relaxation in dysprosium-based 0D and 1D architectures, *Dalton Trans.*, 2018, **47**, 11782.
18 A. Raya-Barón, I. Oyarzabal, F. M. Arrabal-Campos, J. M. Seco, A. Rodríguez-Diéguez and I. Fernández, Dinuclear Coordination Compounds Based on a 5-Nitropicolinic Carboxylate Ligand with Single-Molecule Magnet Behavior, *Inorg. Chem.*, 2017, **56**, 8768.
19 T. Pugh, F. Tuna, L. Ungur, D. Collison, E. J. L. McInnes, L. F. Chibotaru and R. A. Layfield, Influencing the properties of dysprosium single-molecule magnets with phosphorus donor ligands, *Nat. Commun.*, 2015, **6**, 7492.
20 F. Tuna, C. A. Smith, M. Bodensteiner, L. Ungur, L. F. Chibotaru, E. J. L. McInnes, R. E. P. Winpenny, D. Collison and R. A. Layfiled, A High Anisotropy Barrier in a Sulfur-Bridged Organodysprosium Single-Molecule Magnet, *Angew. Chem., Int. Ed.*, 2012, **51**, 6976.
21 J. D. Rinehart, M. Fang, W. J. Evans and J. R. Long, Strong exchange and magnetic blocking in N_2^{3-}-radical-bridged lanthanide complexes, *Nat. Chem.*, 2011, **3**, 538.
22 J. D. Rinehart, M. Fang, W. J. Evans and J. R. Long, A N_2^{3-} Radical-Bridged Terbium Complex Exhibiting Magnetic Hysteresis at 14 K, *J. Am. Chem. Soc.*, 2011, **133**, 14236.
23 S. Demir, M. I. Gonzalez, L. E. Darago, W. J. Evans and J. R. Long, Giant coercivity and high magnetic blocking temperatures for N_2^{3-} radical-bridged dilanthanide complexes upon ligand dissociation, *Nat. Commun.*, 2017, **8**, 2144.
24 F.-S. Guo and R. A. Layfield, Strong direct exchange coupling and single-molecule magnetism in indigo-bridged lanthanide dimers, *Chem. Commun.*, 2017, **53**, 3130.
25 Y.-S. Meng, J. Xiong, M.-W. Yang, Y.-S. Qiao, Z.-Q. Zhong, H.-L. Sun, J.-B. Han, T. Liu, B.-W. Wang and S. Gao, Experimental Determination of Magnetic Anisotropy in Exchange-Bias Dysprosium Metallocene Single-Molecule Magnets, *Angew. Chem., Int. Ed.*, 2020, **59**, 13037.
26 B. M. Day, N. F. Chilton and R. A. Layfield, Molecular and electronic structures of donor-functionalized dysprosium pentadienyl complexes, *Dalton Trans.*, 2015, **44**, 7109.
27 T. Han, Y.-S. Ding, Z.-H. Li, K.-X. Yu, Y.-Q. Zhai, N. F. Chilton and Y.-Z. Zheng, A dichlorido-bridged dinuclear Dy(iii) single-molecule magnet with an effective energy barrier larger than 600 K, *Chem. Commun.*, 2019, **55**, 7930.
28 L. Norel, L. E. Darago, B. L. Guennic, K. Chakarawet, M. I. Gonzalez, J. H. Olshansky, S. Rigaut and J. R. Long, A Terminal Fluoride Ligand Generates Axial Magnetic Anisotropy in Dysprosium Complexes, *Angew. Chem., Int. Ed.*, 2018, **57**, 1933.
29 Y. Huo, Y.-C. Chen, S.-G. Wu, J.-L. Liu, J.-H. Jia, W.-B. Chen, B.-L. Wang, Y.-Q. Zhang and M.-L. Tong, Effect of Bridging Ligands on Magnetic Behavior in Dinuclear Dysprosium Cores Supported by Polyoxometalates, *Inorg. Chem.*, 2019, **58**, 1301.
30 F.-S. Guo, A. K. Bar and R. A. Layfield, Main Group Chemistry at the Interface with Molecular Magnetism, *Chem. Rev.*, 2019, **119**, 8479.
31 L. Ungur and L. F. Chibotaru, Ab Initio Crystal Field for Lanthanides, *Chem. – Eur. J.*, 2017, **23**, 3708.
32 S. K. Langley, C. M. Forsyth, B. Moubaraki and K. S. Murray, A fluoride bridged $\{Cr^{III}_4Dy^{III}_4\}$ single molecule magnet, *Dalton Trans.*, 2015, **44**, 912.
33 Y.-S. Meng, Y.-Q. Zhang, Z.-M. Wang, B.-W. Wang and S. Gao, Weak Ligand-Field Effect from Ancillary Ligands on Enhancing Single-Ion Magnet Performance, *Chem. – Eur. J.*, 2016, **22**, 12724.
34 J. J. Baldoví, J. J. Borrás-Almenar, J. M. Clemente-Juan, E. Coronado and A. Gaita-Ariño, Modeling the properties of lanthanoid single-ion magnets using an effective point-charge approach, *Dalton Trans.*, 2012, **41**, 13705.
35 D. Aravena and E. Ruiz, Shedding Light on the Single-Molecule Magnet Behavior of Mononuclear DyIII Complexes, *Inorg. Chem.*, 2013, **52**, 13770.
36 N. F. Chilton, D. Collison, E. J. L. McInnes, R. E. P. Winpenny and A. Soncini, An electrostatic model for the determination of magnetic anisotropy in dysprosium complexes, *Nat. Commun.*, 2013, **4**, 2551.
37 S.-D. Jiang and S.-X. Qin, Prediction of the quantized axis of rare-earth ions: the electrostatic model with displaced point charges, *Inorg. Chem. Front.*, 2015, **2**, 613.
38 Y.-C. Chen, J.-L. Liu, L. Ungur, J. Liu, Q.-W. Li, L.-F. Wang, Z.-P. Ni, L. F. Chibotaru, X.-M. Chen and M.-L. Tong, Symmetry-Supported Magnetic Blocking at 20 K in Pentagonal Bipyramidal Dy(III) Single-Ion Magnets, *J. Am. Chem. Soc.*, 2016, **138**, 2829.
39 Y.-S. Meng, S.-D. Jiang, B.-W. Wang and S. Gao, Understanding the Magnetic Anisotropy toward Single-Ion Magnets, *Acc. Chem. Res.*, 2016, **49**, 2381.
40 E. M. Pineda, N. F. Chilton, R. Marx, M. Dörfel, D. O. Sells, P. Neugebauer, S.-D. Jiang, D. Collison, J. van Slageren, E. J. L. McInnes and R. E. P. Winpenny, Direct measurement of dysprosium(III)···dysprosium(III) interactions in a single-molecule magnet, *Nat. Commun.*, 2014, **5**, 5243.
41 R. Marx, F. Moro, M. Dorfel, L. Ungur, M. Waters, S. D. Jiang, M. Orlita, J. Taylor, W. Frey, L. F. Chibotaru and J. van Slageren, Spectroscopic determination of crystal field splittings in lanthanide double deckers, *Chem. Sci.*, 2014, **5**, 3287.
42 M. Gysler, F. El Hallak, L. Ungur, R. Marx, M. Hakl, P. Neugebauer, Y. Rechkemmer, Y. Lan, I. Sheikin, M. Orlita, C. E. Anson, A. K. Powell, R. Sessoli, L. F. Chibotaru and J. van Slageren, Multitechnique investigation of Dy_3 – implications for coupled lanthanide clusters, *Chem. Sci.*, 2016, **7**, 4347.

